

## Article

# Combined Energetic and Exergetic Performance Analysis of Air Bubbles Injection into a Plate Heat Exchanger: An Experimental Study

Zakaria M. Marouf <sup>1,\*</sup>  and Mahmoud A. Fouad <sup>2</sup>

<sup>1</sup> Mechanical Engineering Department, Faculty of Engineering and Technology, Future University in Egypt, New Cairo 11835, Egypt

<sup>2</sup> Mechanical Power Engineering Department, Faculty of Engineering, Cairo University, Giza 12613, Egypt

\* Correspondence: zakaria.mustafa@fue.edu.eg

**Abstract:** This paper aims to give a comprehensive energetic-exergetic performance analysis on the impacts of injecting-submillimeter of air bubbles into both sides of cold and hot water streams before the entrance port of a corrugated plate heat exchanger (C-PHE) having ten plates within counterflow configuration. Hence, optimize the energy and exergy effectiveness at different operating conditions for counter and parallel fluid flow configurations. Hot streams were studied in seven flow rates ranging from 280 L/h to 880 L/h with a regular step of 100 L/h, and constant hot water temperature and cold-water stream of 50 °C and 290 L/h, respectively. Hence, the air was discharged with four flow rates ranging between 150 and 840 L/h. The obtained results showed the vital role of the ABI technique in enhancing the NTU and effectiveness by 59% and 18.6%, respectively, for CWS. The entropy generation was reduced to 0.038 W/K and the augmentation entropy generation number to 0.087 at the low airflow rate for CWS, which are the main parameters for evaluating the EGM. These two parameters increase the Witte-Shamsundar-efficiency to a maximum value of 98.6% at the same operating conditions. Moreover, the exergy effectiveness was enhanced to a maximum value of 80.9% at a high ABI flow rate and low volumetric rate of the hot stream at CWS. The thermo-economic assessment has been carried out, which revelers the positive effects of ABI on the combined energetic and exergetic performance on both sides, i.e., hot and cold sides.

**Keywords:** plate heat exchanger; air bubbles injection; entropy generation rate; combined energetic and exergetic performance; thermo-economic assessment



**Citation:** Marouf, Z.M.; Fouad, M.A. Combined Energetic and Exergetic Performance Analysis of Air Bubbles Injection into a Plate Heat Exchanger: An Experimental Study. *Energies* **2023**, *16*, 1164. <https://doi.org/10.3390/en16031164>

Academic Editors: Gianpiero Colangelo and Abderrahmane Bairi

Received: 5 December 2022

Revised: 6 January 2023

Accepted: 17 January 2023

Published: 20 January 2023



**Copyright:** © 2023 by the authors. Licensee MDPI, Basel, Switzerland. This article is an open access article distributed under the terms and conditions of the Creative Commons Attribution (CC BY) license (<https://creativecommons.org/licenses/by/4.0/>).

## 1. Introduction

Heat exchangers (HEs) comprise devices that exchange heat among two or more different fluids. The heat transfer between the fluid is solely based on temperature difference, without the aid of an external energy source. Optimizing the exchanged energy transfer of HE comes from the priority of the researcher for maximizing energy saving and reducing capital costs for better heat exchangers efficiency. They are classified according to their geometries such as plate, extended surface, and tubular. Corrugated plate heat exchangers (C-PHEs) are commonly used in various applications such as automotive, chemical and metal industries, heating and heat recovery, power generation, and food processes. Many research articles concentrate on improving thermal-hydraulic performance using various techniques such as geometry retrofit, inserting nanofluid, and injecting air bubbles.

Khan et al. [1] experimentally investigated the pressure losses for two symmetrical chevron angles of 30°/30°, 60°/60° and non-symmetrical angle of 30°/60° of a PHE. They noticed that the plate of the non-symmetrical chevron angle enhanced the performance more than the other two symmetrical angles did. The maximum pressure losses of 50, 42, and 40 kPa were observed for chevron angles of 60°/60°, 30°/30°, and 30°/60° respectively. Faizal and Ahmed [2] conducted their experimental study on a C-PHE of 20 plates with a

total heat transfer area of 1.163 m<sup>2</sup> and three varying spaces between the plates ranging from 6 to 12 mm to evaluate the best HTR optimally. Their experimental tests were performed with a parallel fluid flow configuration. They concluded that the corrugations on the plates augment turbulence at higher flow rates, which results in improving the HTR. Hence, the optimum HTR was achieved at a minimum plate spacing of 6 mm. Al Zahrani et al. [3] experimentally and numerically performed tests on C-PHE to evaluate the HTR characteristics. Their results showed that the Nusselt number ( $Nu$ ) increases as Reynolds numbers ( $Re$ ) increase and vice versa with the friction coefficient. Another experimental investigation conducted by Attalla and Maghrabie [4] studied the impacts of plate roughness on the performance of a C-PHE has 16 plates. Their findings revealed that the C-PHE effectiveness decreases from 48% to 28% as the mass flow rate increases from 0.08 kg/s to 0.8 kg/s, respectively, for smooth plates. Moreover, the pressure loss ( $\Delta P$ ) and pumping power were increased with increasing the  $Re$ . In addition, they noticed that the rough plate surface enhanced the effectiveness ( $\epsilon$ ) by 11.5% compared to the smooth plates. YANG et al. [5] experimentally demonstrated the effect of flow direction on the thermal performance of Refrigerant R-410A in PHE. The authors found that the evaporation heat transfer coefficient is greater within a parallel-flow configuration than in a counterflow arrangement, while the parallel-flow configuration has a lower overall heat transfer ( $U$ ) performance than the counterflow arrangement. Zhi-Jian et al. [6] presented their experimental and numerical studies about a novel PHE design using unclean working fluid. Their results showed that the new design enhanced the heat transfer rate by 25% compared to the Chevron type. Hence, the new design prevents flow blockage from happening during the use of unclean fluid. Elbarghthi et al. [7] numerically investigated the performance of a PHE using R744 and HFOs as working fluids which use at critical low temperatures. Their work was simulated by MATLAB integrated with the NIST standard database. The authors reported that the evaluated parameters of PHE have an insignificant difference in the number of plates greater than 40 plates. Moreover, the convection coefficient was enhanced by 50% for R1233zd(E) and resulting in increasing the pressure of the hot stream from 10 MPa to 12 MPa.

Numerous studies are exploring the impacts of using various nanofluids at different concentrations in HEs, especially for C-PHEs. Ajeeb et al. [8] used an experimental method to investigate the performance of a PHE using Al<sub>2</sub>O<sub>3</sub> nanoparticles with low concentrations ranging from 0.01% to 0.2% with 0.05 fixed increasing vol.% concentration step. Moreover, the nanoparticles' performance was tested and compared to utilize the ethylene glycol with 15% and 30% concentrations. The reported results showed that HTR was enhanced with increased nanoparticle concentration that reached 27% at 0.2 vol% for distilled water-based Al<sub>2</sub>O<sub>3</sub> nanofluid followed by an increase in  $\Delta P$  by 8%. In addition, the heat transfer enhancement decreased as the ethylene glycol concentration increased based on Al<sub>2</sub>O<sub>3</sub> nanofluid. Çuhadaroğlu and Hacisalihoğlu [9] experimentally evaluated the thermal-hydraulic performance of a PHE using H<sub>2</sub>O/CuO nanofluids with a four-volume fraction. The authors reported that the PHE effectiveness reached a maximum value of 96% at a volume fraction of 0.8 for H<sub>2</sub>O/CuO nanofluids. Furthermore, the lowest thermal efficiency and high pumping power occur at a high-volume fraction of 1.1 which also decreases the PHE effectiveness. The theoretical study presented by Ham et al. [10] examines the effect of various nanofluids based on lithium bromide solution as a working fluid on the thermal performance of a PHE. Their results indicated that nanoparticles have a generally significant impact in improving the thermal performance of the PHE for all utilized nanofluids in this study, especially Al<sub>2</sub>O<sub>3</sub> nanoparticle has a great effect than TiO<sub>2</sub>, Fe<sub>2</sub>O<sub>3</sub>, CuO, and CNT at the same volume concentrations. Bhattad et al. [11] theoretically studied the energetic-exergetic performance of C-PHE having 10 plates utilizing hybrid nanoparticles. Their results showed that HTR was enhanced by 1.44% for hybrid propylene glycol.

On the other hand, PHEs are often utilized for two-phase flow engineering applications such as evaporation or absorption. The ABI technique is used for most types of HEs as a performance enhancement method. Hence, it received great attention, as there is no need

to redesign, reinstall, or retrofit the system. Marouf et al. [12] experimentally investigated the impacts of ABI on the HWS on the performance of C-PHE. Their study arranged with parallel flow direction with seven discharge hot water streams ranging from 280 L/h to 880 L/h and a constant amount of cold water of 290 L/h. Furthermore, the air was injected with four volumetric flow rates ranging between 150 and 840 L/h. The author found that ABI has a great effect on enhancing the NTU ratio by 12.4% and the  $\epsilon$  – Ratio by 14.6%. Zarei et al. [13] experimentally evaluate the helical-coil-heat-exchanger performance utilizing the vapor compression refrigeration cycle on one side and the other side injected air bubbles into the working fluid. Four different tube configurations of ABI were tested with airflow rates ranging from 180 to 660 L/h. It was noticed that the optimum airflow rate was 540 L/h and the coefficient of performance for the refrigeration cycle improved by 124%. Furthermore, the  $Nu$  was enhanced by 452% for the case of ABI compared with the original case (without ABI). Marzouk et al. [14] conducted their experimental study to study the effects of injected air bubbles on the thermo-hydraulic performance of a shell-and-tube-heat exchanger. In their study, the shell fluid volume flow rate was kept constant at 1080 L/h and the tube side volume ranged between 840 and 960 L/h. Furthermore, the air was injected into the tube side with three different amounts ranging from 60 to 180 L/h and two configurations. Their results showed that the performance parameters were enhanced from 1% to 23% for injected air bubbles inside the inserted tube. Asano et al. [15] visualized a two-phase flow using thermal neutron radiography for a PHE. They observed that the entrance ports of PHE have bad effects on the flow behavior of the mixed two-phase. Furthermore, more research is required to improve the design of the inlet ports. Another three experimental studies were carried out by Buscher [16–18] to visualize and simulate the flow pattern of two-phase flow in C-PHE. In this work [16] and related references, edge detection was used to separate large bubble clusters and texture analysis identified the local film and bubbly flow. This method was appropriate for locally inhomogeneous two-phase flow that is difficult to visualize. According to his investigation [18], the centrifugal force has a great effect on the flow direction of two-phase flow which circumvents the channel corrugations concerning the buoyancy force. Hence, He observed that the effects of flow direction on two-phase flow in both cases of a dominant centrifugal and dominant buoyancy were small to negligible and significant on the mean diameter, respectively [17]. Lee et al. [19] conducted their experimental work to evaluate the pressure losses of inlet and outlet ports for single-phase and two-phase R1234ze(E) flows inside PHE. They noted that the gravity and flow direction notably influences the port pressure loss due to the non-uniformity of flow distribution of two-phase flow.

However, the ABI technique proves its superiority as an effective method for heat transfer enhancement in several types of HEs, there is only a recent experimental study has been conducted for investigating the combined energetic-exergetic performance of a PHE. Furthermore, there are no attempts to compare ABI on both sides of water streams (HWS and CWS) with different fluid directions, i.e., counter and parallel flows. However, the recent investigation that focuses on studying the energetic and exergetic performance of C-PHE presented by Marouf et al. [12] deals with ABI into the HWS with a parallel flow arrangement. Moreover, few research papers focus on the mechanisms of heat transfer due to ABI in PHE using visualization and simulation techniques without addressing the impacts on the energetic-exergetic performance of PHE [15–19].

Efforts were taken in this study to investigate the impacts of ABI on both sides of water streams, i.e., CWS and HWS on the combined energetic-exergetic performance of C-PHE with a counterflow configuration. Moreover, compare the obtained results with the recently studied work [12] for the same C-PHE in the same operating conditions with a parallel fluid flow configuration. Hence, optimize the energy and exergy effectiveness using optimization techniques in order to identify the optimal operating conditions while injecting ABI.





**Figure 2.** Experimental setup components consist of (1) CWB, (2) HWB, (3) C-PHE, and (4) corrugated plate channel of PHE.

**Table 1.** C-PHE technical specifications.

Parameter	Specification
Model	GCP-008-PI
C-PHE Material	1.4401-stainless-steel
Gasket Material (hot/cold)	NBR (Clip-on)
Number of Plates, $N_p$	10 plates
Number of cold-water channels, $N_c$	5 channels
Number of hot water channels, $N_h$	4 channels
Total high, $H$	774 mm
Total width, $L_w$	180 mm
Total Area, $A_t$	4.954 m <sup>2</sup>
Heat transfer area, $A$	0.6 m <sup>2</sup>
Max. operating pressure, $P_{max}$	1 MPa
Max. operating temperature, $T_{max}$	373 K

An air compressor utilizes to inject air into the mixing chamber that was manufactured by the BOYU model (ACQ-003) with a maximum flow rate of 3000 L/h. In addition, the air pressure transducer, control valves, and YF-S201 hall effect air sensor were used for measuring the airflow rate connected to Arduino Uno and calibrated by measuring the output signal using a stethoscope.

### Experimental Procedure

Water was heated to the desired temperature of 50 °C by the means of an HWB that has two heaters connected to a thermistor for temperature control purposes. In addition, a temperature inductor to visualize the heated water temperature inside the storage tank. A circulating pump was used to pump the hot water to the mixing chamber and then to the C-PHE.

Air was injected into the mixing chamber via an air compressor, valve regulators were used for controlling the amount of airflow rate, which was measured using YF-S201 with  $\pm 3\%$  accuracy. Moreover, the schematic diagram for the mixing chamber illustrated in Figure 3 has three ports used depending on whether air bubbles were injected in a side of the two tested water sides (CWS or HWS) cold/hot water inlet, air inlet, and cold/hot water exit. A small air inlet tube of 6.5 mm has  $\sim 30$  tiny holes equally distributed, a pressure transducer, and a digital airflow rate sensor.

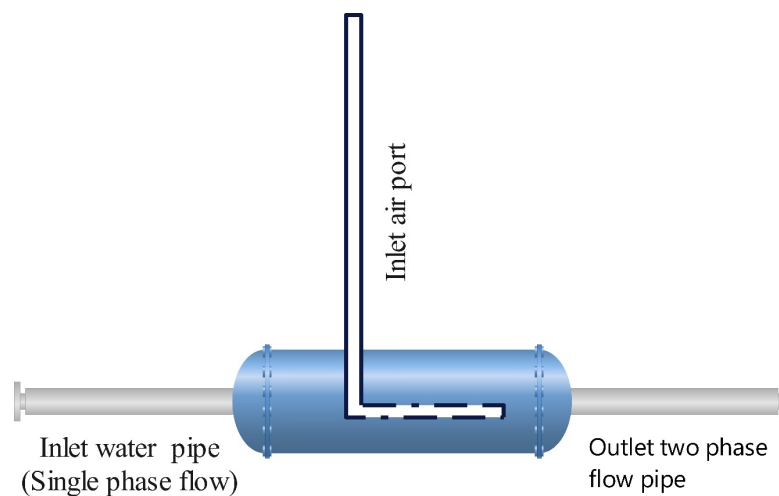


**Figure 3.** Schematic diagram for the mixing chamber.

The chiller refrigerating cycle cools down the heated water coming from C-PHE to the desired low temperature using the CWB. The circulating pump is pumped cold water to the mixing chamber through supplied pipelines to the C-PHE. Hence, there are two thermocouples used for measuring the feed and return water temperature for each bench water. The variable area flow meter (rotamer) is used to measure the volumetric flow rate of cold water with a maximum error of  $\pm 0.5\%$ .

The C-PHE contains a differential pressure transducer with a maximum operating pressure of 100 kPa and two digital flow meters for inlet hot and cold-water type Endress + Hauser model (PROMAG-10H15) with a calibrated maximum error of  $\pm 2.5$  L/h to double-check the obtained volumetric flow rate.

### 3. Data Analysis

In this section, brief data analyses are presented for this investigation based on the first and second laws of thermodynamics. The combination of the first and second laws of thermodynamics includes the entropy generation rate ( $\dot{S}_{gen}$ ) and exergy destruction rate ( $\dot{E}x_{des}$ ) which are widespread in recent decades and are essential for evaluating the performance of a C-PHE [20].

The dimensionless Reynolds number ( $Re_{ch}$ ) for C-PHE channels is the ratio of inertia forces to the viscous shear force that can be computed as follows:

$$Re_{ch} = \frac{\dot{m} D_h}{\mu N_{ch} b L_w} \quad (1)$$

where

$$D_h = 2b \quad (2)$$

where,  $D_h$  is the hydraulic diameter and  $b$  is the corrugation depth that can be obtained from Equation (2) [21] and  $N_{ch}$  is the number of (cold/hot) channels.

We started by investigating the overall heat transfer coefficient ( $U$ ) as follows:

$$U = \frac{\dot{Q}_{avg}}{A \Delta T_{LM}} \quad (3)$$

$$\dot{Q}_{avg} = \frac{\dot{Q}_c + \dot{Q}_h}{2} \quad (4)$$

where

$$\dot{Q}_h = \dot{m}_h c_h (T_{h,i} - T_{h,o}) \text{ and } \dot{Q}_c = \dot{m}_c c_c (T_{c,o} - T_{c,i}) \quad (5)$$

$$\Delta T_{LM} = \frac{(\Delta T_2 - \Delta T_1)}{\ln\left(\frac{\Delta T_2}{\Delta T_1}\right)} \quad (6)$$

$$\Delta T_1 = T_{h,i} - T_{c,i} \text{ and } \Delta T_2 = T_{h,o} - T_{c,o} \quad (7)$$

$$\Delta T_1 = T_{h,i} - T_{c,o} \text{ and } \Delta T_2 = T_{h,o} - T_{c,i} \quad (8)$$

The involved Equations (7) and (8) are used for calculating the temperature difference across the C-PHE inlet and outlet ports for parallel and counter flow directions, respectively.

The  $NTU$  is the second important parameter used for summarizing the combination of  $A$ ,  $U$ , and,  $C_{min}$  which can be obtained from Equation (9) as follows:

$$NTU = \frac{A U}{C_{min}} \quad (9)$$

$$C_{min} = (\dot{m} c)_{min} = \min(\dot{m}_h c_h \text{ or } \dot{m}_c c_c) \quad (10)$$

The equation that describes the effectiveness ( $\varepsilon$ ) of C-PHE is the third important parameter and is defined as the ratio of the actual HTR to the maximum heat transfer rate, illustrated in Equation (11):

$$\varepsilon = \frac{\dot{Q}_{act}}{\dot{Q}_{max}} \quad (11)$$

where,

$$\dot{Q}_{max} = C_{min}(T_{h,i} - T_{c,i}) \quad (12)$$

The heat transfer process between hot and cold streams results in some heat losses which prevent the process to return to its initial state. The heat losses during the operation of HEs are divided into three types such as exchanged heat loss, fluid friction loss, and surrounding losses [22]. The entropy generation  $\dot{S}_{gen}$  implies the irreversibility rate in the processes that are divided into two terms, namely, thermal and friction entropy generation, which are illustrated below in Equation (13). The fluid friction terms in the equation for hot and cold streams may be neglected as a result of values fluctuation as two-phase has fluid streams as air bubbles were injected into water [23]; also, their value is very small compared to the thermal entropy generation with a value not exceeding 0.3% [24]. Furthermore, authors are disregarded during their work analysis [25]. The dimensionless augmentation entropy generation number ( $N_{s,aug}$ ) is the most frequently utilize criterion,

while the EGM criterion has been used to model and optimize HEs design and can be calculated from Equation (14) [20,26].

$$\dot{S}_{gen} = \dot{m}_c c_c \ln\left(\frac{T_{c,o}}{T_{c,i}}\right) + \dot{m}_h c_h \ln\left(\frac{T_{h,o}}{T_{h,i}}\right) + \frac{\dot{m}_c}{\rho_c} \Delta P_c \frac{\ln\left(\frac{T_a}{T_{c,i}}\right)}{T_a - T_{c,i}} + \frac{\dot{m}_h}{\rho_h} \Delta P_h \frac{\ln\left(\frac{T_a}{T_{h,i}}\right)}{T_a - T_{h,i}} \quad (13)$$

$$N_{s, aug} = \frac{\dot{S}_{gen,sp}}{\dot{S}_{gen,tp}} \quad (14)$$

The entropy generation number ( $N_s$ ) is a dimensionless number which is the ratio of entropy generation rate to the minimum heat capacity and can be calculated as:

$$N_s = \frac{\dot{S}_{gen}}{C_{min}} \quad (15)$$

Exergy destruction rate ( $\dot{E}x_{des}$ ) is defined as the maximum useful energy that a system can undergo in a given environment. The rate of exergy destruction can be calculated as:

$$\dot{E}x_{des} = T_a \dot{S}_{gen} \quad (16)$$

Witte-Shamsundar efficiency ( $\eta_{W-S}$ ), is an important principle for evaluating the combined energetic and exergetic performance of HEs [27,28]

$$\eta_{W-S} = 1 + \frac{T_a}{\frac{T_{h,i} + T_{h,o}}{2}} - \frac{T_a}{\frac{T_{c,i} + T_{c,o}}{2}} \quad (17)$$

The exergy effectiveness ( $\varepsilon_{ex}$ ) was introduced by Bruges and Reistad [24,29], which is used to quantify the HEs irreversibility in terms of exergy gained by the cold water and the exergy offered by the hot water.

$$\varepsilon_{ex} = \pm \frac{\dot{m}_c c_c \left[ T_{c,o} - T_{c,i} - T_a \ln\left(\frac{T_{c,o}}{T_{c,i}}\right) \right]}{\dot{m}_h c_h \left[ T_{h,o} - T_{h,i} - T_a \ln\left(\frac{T_{h,o}}{T_{h,i}}\right) \right]} \quad (18)$$

### Uncertainty Analysis

The uncertainties analysis was performed for the tested parameters to estimate the error in the obtained results during the measuring process by different measurement devices while conducting the tests using Kline and McClintock method [30] as follows and tabulated in Table 2.

**Table 2.** Computed parameters uncertainty.

Parameter	Symbol	Uncertainty
Inlet/outlet chilled water temperatures	$T_{c,i}, T_{c,o}$	$\pm 0.15$ °C
Inlet/outlet heated water temperatures	$T_{h,i}, T_{h,o}$	$\pm 0.15$ °C
Chilled and heated water volume flow rate	$Q_c, Q_h$	$\pm 0.5\%$
Mass flow rate	$\dot{m}_h, \dot{m}_c$	$\pm 0.51\%$
Volumetric airflow rate	$Q_{air}$	$\pm 3$ L/h
Overall heat transfer coefficient	$U$	$\pm 0.04862$ kW/m <sup>2</sup> · °C
Effectiveness	$\varepsilon$	$\pm 5.53\%$
Effectiveness Ratio	$\varepsilon - Ratio$	$\pm 5.53\%$
Number of transfer units	$NTU$	$\pm 5.13\%$
NTU- Ratio	$NTU - Ratio$	$\pm 6.10\%$
Entropy generation rate	$\dot{S}_{gen}$	$\pm 10.30\%$
Entropy generation number	$N_s$	$\pm 10.46\%$

Table 2. Cont.

Parameter	Symbol	Uncertainty
Augmentation entropy generation rate	$N_{s,avg}$	$\pm 11.20\%$
Exergy destruction rate	$\dot{E}x_{des}$	$\pm 10.45\%$
Witte-Shamsundar efficiency	$\eta_{W-S}$	$\pm 0.78\%$
Exergy effectiveness	$\varepsilon_{ex}$	$\pm 1.35\%$
Net profit per unit transfer load	$\eta_p$	$\pm 10.92\%$
Density, and Specific heat capacities for water	$\rho, c$	$\pm(0.1-0.15)\%$

Effectiveness uncertainty ( $\omega_\varepsilon$ ) can be estimated from Equation (19) and derived from Formulas (20) and (21).

$$\omega_\varepsilon = \left[ \left( \frac{\partial \varepsilon}{\partial \dot{Q}_{act}} \omega_{\dot{Q}_{act}} \right)^2 + \left( \frac{\partial \varepsilon}{\partial \dot{Q}_{max}} \omega_{\dot{Q}_{max}} \right)^2 \right]^{1/2} \quad (19)$$

$$\frac{\partial \varepsilon}{\partial \dot{Q}_{act}} = \frac{1}{\dot{Q}_{max}} \quad (20)$$

$$\frac{\partial \varepsilon}{\partial \dot{Q}_{max}} = \frac{-\dot{Q}_{act}}{\dot{Q}_{max}^2} \quad (21)$$

Overall heat transfer coefficient uncertainty  $\omega_U$  can be obtained from Equation (22) and derived from (23) to (25).

$$\omega_U = \left[ \left( \frac{\partial U}{\partial \dot{Q}_{avg}} \omega_{\dot{Q}_{avg}} \right)^2 + \left( \frac{\partial U}{\partial A} \omega_A \right)^2 + \left( \frac{\partial U}{\partial \Delta T_{LM}} \omega_{\Delta T_{LM}} \right)^2 \right]^{1/2} \quad (22)$$

$$\frac{\partial U}{\partial \dot{Q}_{avg}} = \frac{1}{A \Delta T_{LM}} \quad (23)$$

$$\frac{\partial U}{\partial A} = \frac{-\dot{Q}_{avg}}{A^2 \Delta T_{LM}} \quad (24)$$

$$\frac{\partial U}{\partial \Delta T_{LM}} = \frac{-\dot{Q}_{avg}}{A \Delta T_{LM}^2} \quad (25)$$

NTU uncertainty ( $\omega_{NTU}$ ) can be calculated as follows:

$$\omega_{NTU} = \left[ \left( \frac{\partial NTU}{\partial A} \omega_A \right)^2 + \left( \frac{\partial NTU}{\partial U} \omega_U \right)^2 + \left( \frac{\partial NTU}{\partial C_{min}} \omega_{C_{min}} \right)^2 \right]^{1/2} \quad (26)$$

where,

$$\frac{\partial NTU}{\partial A} = \frac{U}{C_{min}} \quad (27)$$

$$\frac{\partial NTU}{\partial U} = \frac{A}{C_{min}} \quad (28)$$

$$\frac{\partial NTU}{\partial C_{min}} = \frac{-AU}{C_{min}^2} \quad (29)$$

#### 4. Results and Discussion

This section discusses the obtained results from the experimental tests and compared them with the previously published article authored by Marouf et al. [12]. Air was injected in four amounts ( $Q_{air}$ ) of 150 L/h, 350 L/h, 630 L/h, and 840 L/h into CWS and HWS and seven ( $Q_h$ ) varies from 280 to 880 L/h with an increasing flow step of 100 L/h, which corresponds to the channel Reynolds number ( $Re_{ch}$ ) of 391, 530, 670, 809, 949, 1088, and 1227. Moreover, a fixed hot temperature and cold-water flow rate of 50 °C and 290 L/h, respectively, that has a corresponding  $Re_{ch}$  of 224, respectively. Marouf et al. [12] studied the aforementioned tested parameters for parallel flow configuration with ABI into HWS without comparing their results for the case of ABI into CWS. The following terminology is used to facilitate calling the performed experimental test cases:

1. Case 0: Original case (without ABI)
2.  $Q_{air} = 150c$ : ABI-CWS with 150 L/h
3.  $Q_{air} = 150h$ : ABI-HWS with 150 L/h
4.  $Q_{air} = 350c$ : ABI-CWS with 350 L/h
5.  $Q_{air} = 350h$ : ABI-HWS with 350 L/h
6.  $Q_{air} = 630c$ : ABI-CWS with 630 L/h
7.  $Q_{air} = 630h$ : ABI-HWS with 630 L/h
8.  $Q_{air} = 840c$ : ABI-CWS with 840 L/h
9.  $Q_{air} = 840h$ : ABI-HWS with 840 L/h

The NTU and effectiveness ( $\epsilon$ ) were increased significantly with the counter-flow direction with maximum values of 2.996 and 0.906, respectively, compared with parallel flow arrangements that have maximum values of 2.219 and 0.707, respectively, for the original case (without ABI) as illustrated in Figure 4. This indicates that the counter-flow configuration generally has a great thermal performance as the hot and cold water moves in opposite directions. More exchanged energy is transferred, which increases the cold water exit temperature rather than in the parallel flow configuration. However, the low thermal performance in the parallel flow direction, many engineering applications required used flow configuration in the C-PHE. Furthermore, the pressure drop ( $\Delta P$ ) across hot water of C-PHE was investigated for both flow directions as depicted in Figure 5. The obtained results showed that the hot water in the counter-flow direction has a maximum  $\Delta P$  of 19 kPa at  $Q_h = 880$  L/h and  $\Delta P = 14.2$  kPa at the same flow rate, for parallel flow direction. This indicates that the fluid flow within the counter-flow direction has bad hydraulic performance over the parallel fluid flow direction for the original case.

##### 4.1. Energetic Performance Analysis

In this section, the authors discuss the energetic performance of a C-PHE that includes the analysis of effectiveness,  $\epsilon$  – Ratio, NTU, and NTU Ratio at different operating conditions.

##### 4.1.1. Effectiveness and Effectiveness Ratio Analysis

Numerous experimental tests were carried out to evaluate the thermal performance of C-PHE for ABI on both HWS and CWS. The demonstrated results shown in Figure 6a indicate that  $\epsilon$  increases from 0.651 to 0.906 at  $Q_h$  ranging from 280 L/h to 880 L/h for the original case (Case 0). Injected air bubbles into a CWS have superior effects on the  $\epsilon$  that reached 0.989 for  $Q_{air} = 150 c$  at  $Q_h = 880$  L/h compared to a maximum value of  $\epsilon$  of 0.957 for  $Q_{air} = 630 h$  at  $Q_h = 880$  L/h with counter flow arrangement. The curves 630 h and 840 h intersect at high flow rates because air injecting air bubbles with high flow rates inside C-PHE increases the turbulence intensity and the mixing thermal boundary layer of fluid which results in augmented HTR. Comparing the obtained results of ABI into the HWS to the previous work [12] under the same operating conditions, the authors noticed that the maximum  $\epsilon = 0.792$  occurs at  $Q_{air} = 630$  L/h and  $Q_h = 880$  L/h within the inflow direction. This indicates that the ABI has great thermal effects within the counter-flow rather than the parallel flow arrangement, especially in the CWS.

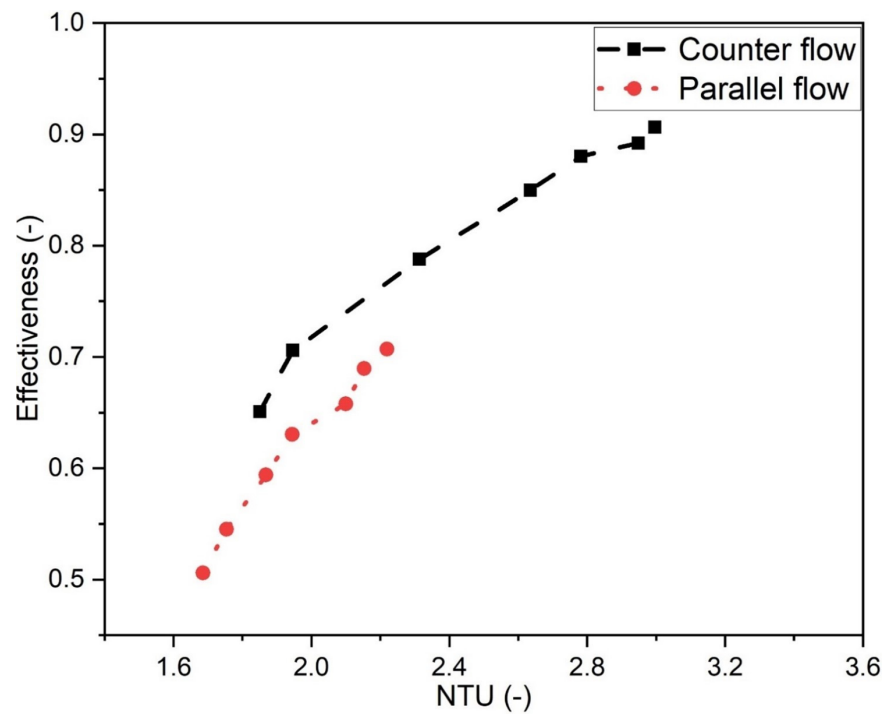


**Figure 4.** Effectiveness vs. NTU for the original case of C-PHE with counter and parallel fluid flows arrangement.

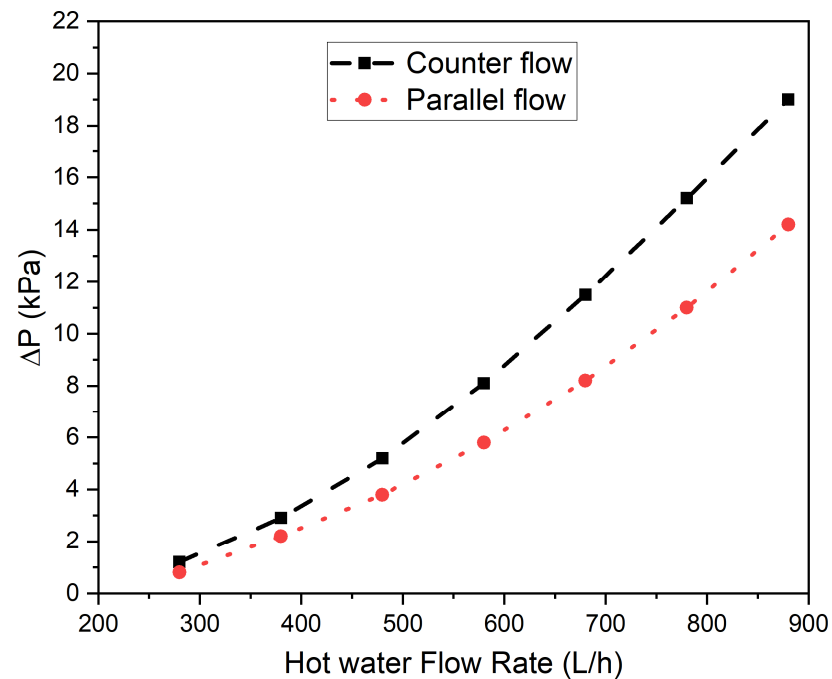


**Figure 5.** The relationship between pressure losses ( $\Delta P$ ) and counter and parallel hot water flow rates at the original case.

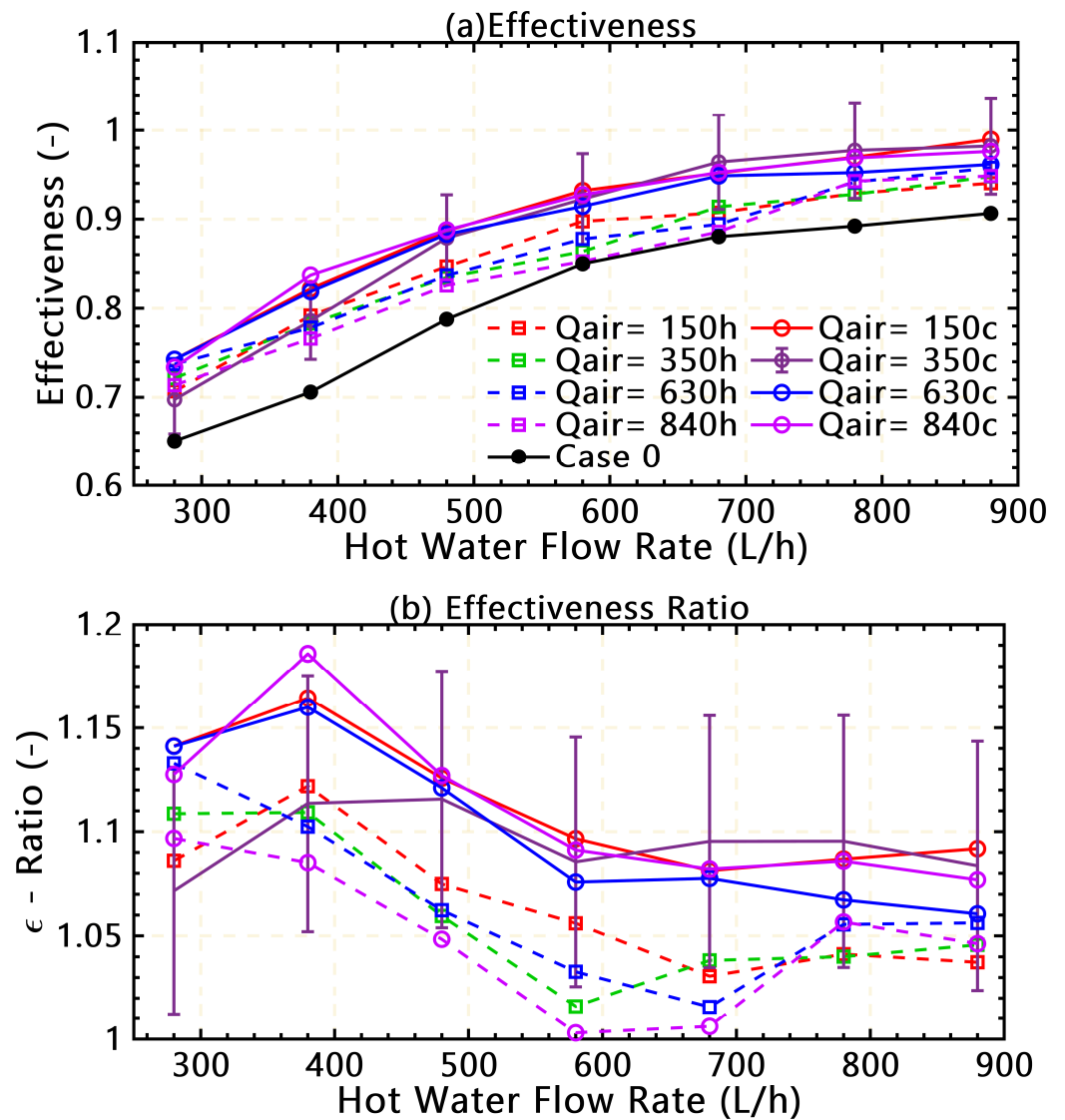


**Figure 6.** (a) Effectiveness and (b)  $\epsilon - Ratio$  vs. hot water flow rates at different operating conditions for single-phase, and two-phase flow of ABI into CWS and HWS.

Effectiveness ratio ( $\epsilon - Ratio$ ) is the newly investigated parameter that represents the ratio of  $\epsilon$  of the single phase to the  $\epsilon$  of the two-phase flow and can be calculated as illustrated in Equation (30).

$$\epsilon - Ratio = \frac{\epsilon_{tp}}{\epsilon_{sp}} \tag{30}$$

The  $\epsilon - Ratio$  was enhanced with a maximum value of 1.186 at  $Q_{air} = 840$  L/h and  $Q_h = 880$  L/h and 1.133 at  $Q_{air} = 630$  L/h and  $Q_h = 280$  L/h, for ABI into CWS and HWS, respectively, as shown in Figure 6b. Furthermore, the  $\epsilon - Ratio$  for ABI in both cases have the same trend with great thermal enhancement. In addition, comparing these results with the previously studied  $\epsilon - Ratio$  reached a maximum value of 1.146 at  $Q_{air} = 350$  L/h and  $Q_h = 280$  L/h within parallel flow configuration which is greater than the present study value. Although the value of  $\epsilon - Ratio$  was greater in the previous work, the enhancement was greater at the other operating conditions with the counter flow direction. These enhancements in  $\epsilon - Ratio$  result in an increase in HTR significantly at different ABI.

#### 4.1.2. NTU and NTU Ratio Analysis

Figure 7a outlines another important parameter (NTU) which expresses the amount of HTR as a dimensionless number that affects the thermal performance of C-PHE. For the original case, NTU increases from 1.85 to 2.996 as  $Q_h$  increased from 280 to 880 L/h, respectively. For ABI into CWS, NTU increases at a low ABI of  $Q_{air} = 150$  L/h with a maximum value of 2.76 to 4.03 at  $Q_h$  ranged from 280 to 880 L/h, respectively. Hence, ABI into HWS, NTU increased significantly at  $Q_{air} = 350$  L/h from about 2.35 to 3.11 at  $Q_h$  ranged from 280 to 880 L/h, respectively. We can notice that the effects of ABI on enhancing the HTR for CWS are the greatest compared with ABI in HWS. This thermal enhancement is due to the large-scale mixing of cold water and ABI as the distance between the mixing chamber and the C-PHE entrance port is greater than 0.7 m [28]. In addition, as the air bubbles approach the C-PHE wall the heat transfer boosts as the plate corrugations act as bluff bodies [31].

A new parameter was introduced as a ratio of NTU for two-phase to single-phase flows called *NTU Ratio* as illustrated in Equation (31). Figure 7b shows the remarkable increases in the NTU Ratio that reached a maximum value of 1.59 at  $Q_{air} = 840$  L/h and  $Q_h = 380$  L/h, for ABI into CWS. Hence, this superiority continuo at the same  $Q_h$  at different ABI of 630 and 150 L/h that reached a maximum NTU Ratio of 1.57 for both airflows. For HWS, NTU Ratio reached its maximum value of 1.32 at  $Q_{air} = 630$  L/h and  $Q_h = 280$  L/h then decreases to 1.021 at low  $Q_h = 880$  L/h. The same trend is repeated at the other airflow rates with NTU Ratio decreasing at high  $Q_h$  ranged from 580 to 880 L/h, which indicates the superiority of ABI in CWS for all cases even high  $Q_h$ . Injecting bubbles with a proper size affect significantly enhanced HTR that results in an increasing the NTU by 59%.

$$NTU \text{ Ratio} = \frac{NTU_{tp}}{NTU_{sp}} \quad (31)$$

#### 4.2. Exergetic Performance Analysis

In this section, the exergetic performance according to the second law analysis is discussed briefly as follows:

##### 4.2.1. Entropy Generation Rate Analysis

Figure 8 gives an example of the entropy generation rate ( $\dot{S}_{gen}$ ) that has been investigated for the original case and with different ABI into both CWS and HWS.  $\dot{S}_{gen}$  has a maximum value at  $Q_h = 280$  L/h for all the tests conditions;  $\dot{S}_{gen} = 0.809$  W/K for original case;  $\dot{S}_{gen} \sim 0.76$  W/K at  $Q_{air}$  of 350, 630, and 840 L/h for CWS;  $\dot{S}_{gen} = 1.33$  W/K at  $Q_{air} = 150$  L/h for HWS. A better quality of energy transfer can be achieved with a minimum  $\dot{S}_{gen}$  that is associated with minimum irreversibility. The EGM is a good indicator of the HTR. In addition,  $\dot{S}_{gen}$  is used for evaluating the  $N_{s,avg}$  which is a very important parameter.

##### 4.2.2. Entropy Generation Number Analysis

Consider Figure 9 which demonstrates the dimensionless entropy generation number ( $N_s$ ) that is prevalently used for EGM in order to minimize irreversibility that is required as the relation between  $\Delta T$  and HTR.  $N_s$  reached its maximum value of 0.00255 at  $Q_h = 280$  L/h for (case 0) compared to the ABI into CWS that has a maximum value of about 0.00237 at  $Q_{air}$  of 350, 630, and 840 L/h. Hence, at  $Q_h$  of 380 and 480 L/h the same trend of increased  $N_s$  values until averaged between the remaining hot flow rates at different ABI. Furthermore, the best performance of ABI into CWS has been achieved at  $Q_{air} = 630$  L/h for all operating conditions with minimum values of  $N_s$  even compared to the original case. This performance reflects the positive effect of ABI in enhancing the quality of energy transferred. Comparing these results to the previously published

study, the  $N_s$  for ABI into HWS with counter flow direction has minimum values at all testing conditions.

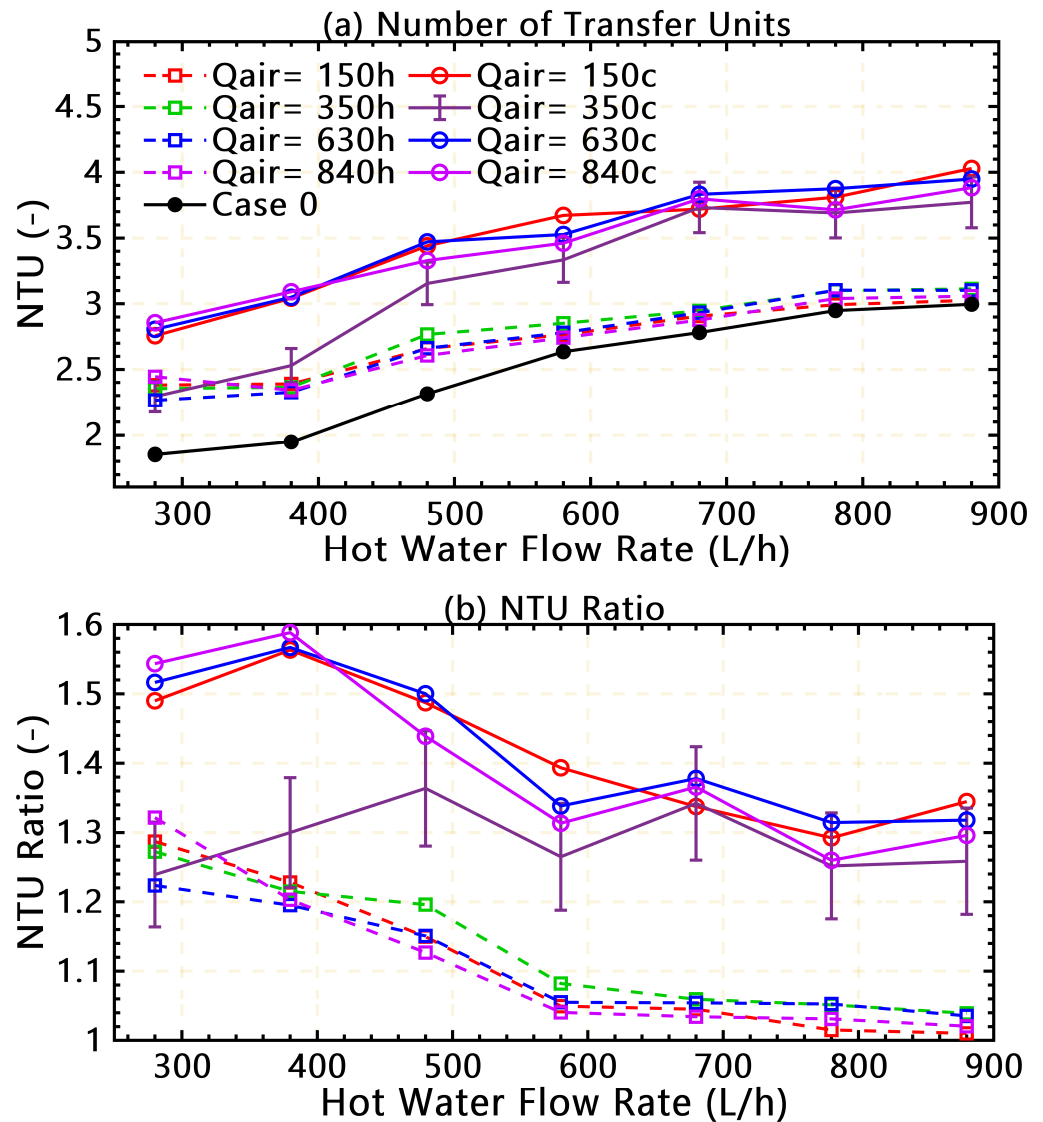


Figure 7. Relationship between (a) NTU and (b) NTU Ratio vs.  $Q_h$  at different operating conditions for the original case (without ABI); and with ABI into CWS, HWS.

#### 4.2.3. Augmentation Entropy Generation Number Analysis

The relationship between  $N_{s, aug}$  and  $Q_h$  at different ABI for both CWS and HWS can be founded in Figure 10. The value of  $N_{s, aug}$  which is below one is the preferred from the thermodynamics point of view. These criteria are established in this study at  $Q_{air} = 630$  L/h at all tested flow rates for ABI into CWS. Hence, all the values of  $N_{s, aug}$  with the acceptable limits except for  $Q_{air} = 350$  L/h at  $Q_h = 680$  L/h reached a maximum value of 4.25. Additionally, the trend is accomplished in the case of ABI into HWS, and most  $N_{s, aug}$  values are below two except four values at a high  $Q_h$  that may be due to the bubble collision that results in configure separation zones between the hot plate surfaces, thus resulting in an evacuation of part of the surface area from hot water. Comparing these results with ABI into HWS with the parallel flow, we can notice that the  $N_{s, aug}$  has a maximum value compared to ABI into HWS with the counter-flow arrangement, which negatively affects the quality of HTR.

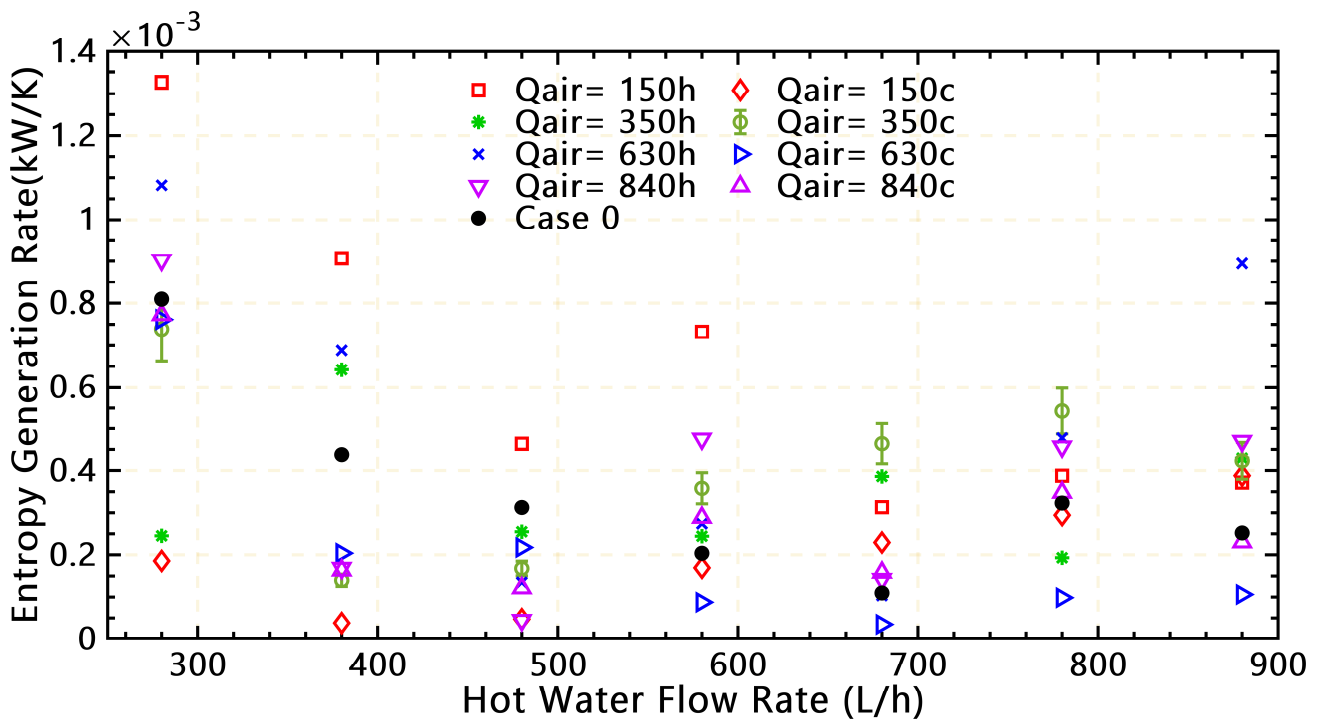


Figure 8. Variations between  $\dot{S}_{gen}$  and  $Q_h$  for original case and different ABI of: CWS; HWS.

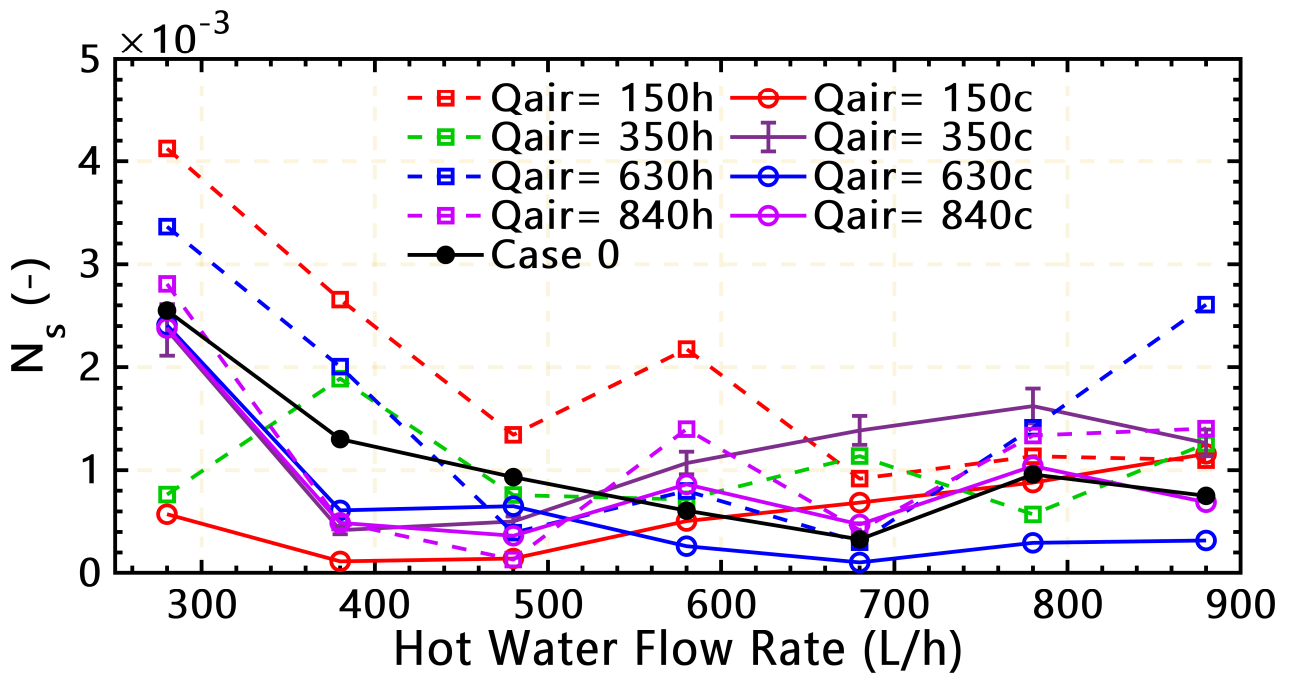


Figure 9. Relationship between  $N_s$  and  $Q_h$  at different operating conditions without/with ABI.

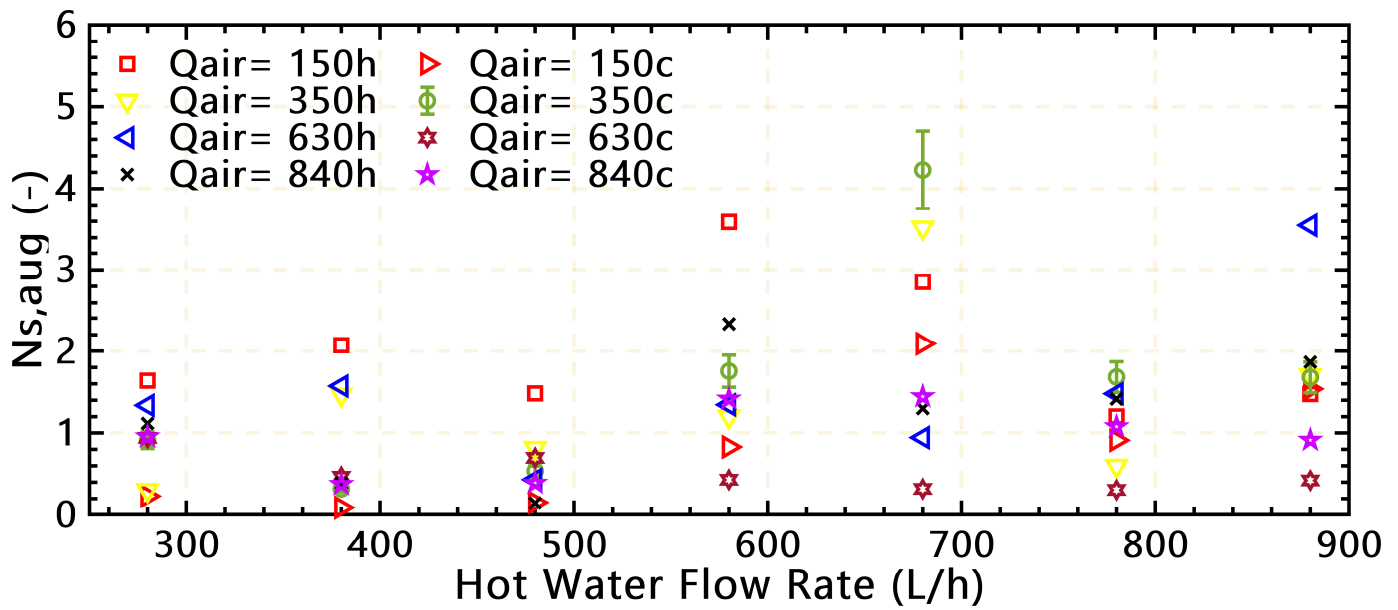


Figure 10.  $N_{s,aug}$  vs.  $Q_h$  at different ABI into both CWS and HWS.

#### 4.2.4. Exergy Destruction Rate Analysis

Thermal exergy destruction rate at different  $Q_h$  for the original case and ABI into CWS and HWS illustrated in Figure 11. The  $\dot{Ex}_{des}$  has high rates at the low volumetric of hot water of 280 L/h at different operating conditions that reached 241.18 W, 230.3 W, and 395.1 W at (case 0), ABI of  $Q_{air} = 350c$ , 630c, and 840c, and ABI of  $Q_{air} = 150$  h, respectively. Hence, for low hot flow rates, the favorable performance of injecting air occurs at  $Q_{air} = 150$  L/h for CWS at  $Q_h$  ranging between 280 L/h to 580 L/h which  $\dot{Ex}_{des}$  reaches its minimum values that ranged between 55.4 W to 13.25 W which is lower than the original case. This result indicates that most of the energy available is transferred to useful heat which strongly affects the performance of C-PHE and enhanced HTR. The noticeable rapid increase in  $\dot{Ex}_{des}$  at curve 630h for the high hot water flow rate is due to injecting air bubbles with a great amount of 630 L/h into HWS that increases the turbulence intensity and irreversibility which is responsible for increasing the  $\dot{Ex}_{des}$ .

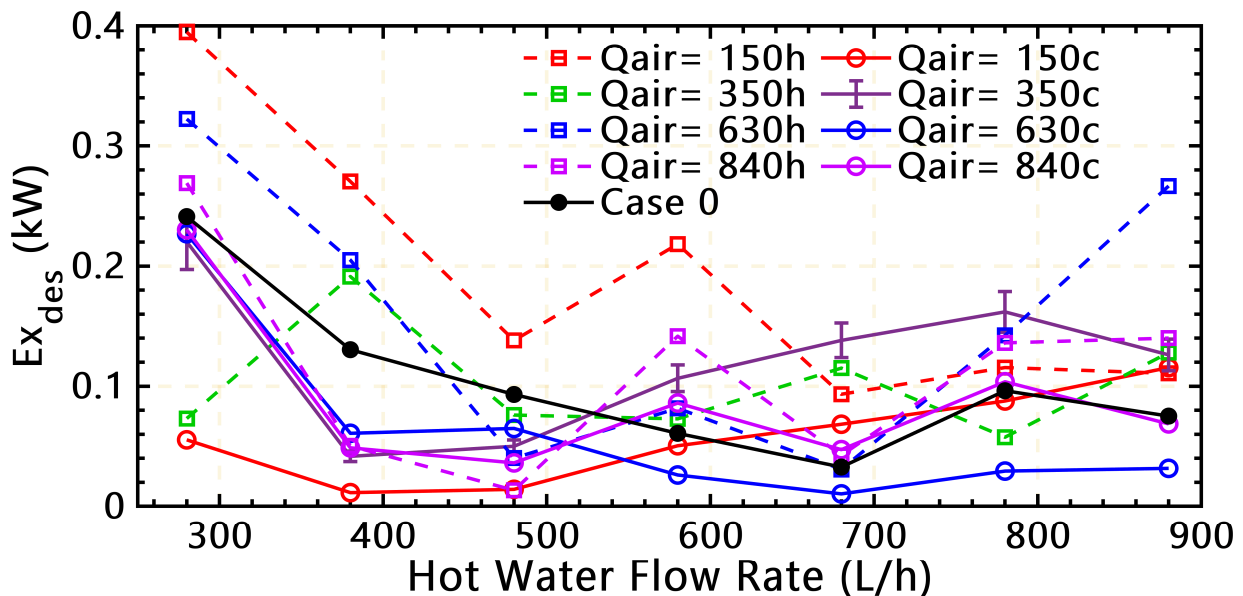


Figure 11.  $\dot{Ex}_{des}$  vs.  $Q_h$  for original cases and different ABI into CWS and HWS.

### 4.3. Combined Energetic-Exergetic Performance Analysis

#### 4.3.1. Exergy Effectiveness

ABI into CWS has great effects on exergy effectiveness ( $\epsilon_{ex}$ ) for all operating conditions especially at low  $Q_{air}$  of 150 L/h for  $Q_h$  ranging from 280 to 580 L/h that are reached about 0.778, then drops at high  $Q_h$  ranged from 680 to 880 L/h to 0.752 as shown in Figure 12. ABI enhanced the  $\epsilon_{ex}$  with a maximum value of 0.809 at  $Q_{air} = 840$  L/h and  $Q_h = 280$  L/h into CWS compared to 0.774 at the same operating conditions in the case of ABI into HWS. Moreover, it shows the superiority of ABI in enhancing the quality of energy transfer and the effectiveness of C-PHE compared to the case without ABI. For ABI into HWS, almost all the tests haven't enhanced the  $\epsilon_{ex}$  compared to the original case, there was a clear improvement in only two cases of ABI at  $Q_{air} = 350$  and 840 L/h low  $Q_h$  compared to the original case. This may be due to the large number of bubbles that vanishes with hot water, especially at high  $Q_h$  that result in energy destruction. Marouf et al.'s [12] results showed the same trend of fluctuated values at different operating conditions of ABI into HWS with parallel flow arrangement.

#### 4.3.2. Witte-Shamsundar Efficiency

The efficiency of energy usage can be evaluated using Witte-Shamsundar efficiency according to the second law analysis, as depicted in Figure 13. ABI has superiority in enhancing the efficiency of all the testing conditions with a maximum value of 0.986 for  $Q_{air} = 150$  L/h and  $Q_h = 380$  L/h into CWS, at this tested condition the entropy generation rate has a minimum value of 0.0382 W/K. Furthermore, these effects are extended also to ABI into HWS but with deterioration at high  $Q_h$  of 880 L/h. Although the maximum improvement in of  $\eta_{W-S}$  that reached its maximum value of 0.983 at  $Q_{air}$  of 840 L/h and  $Q_h = 280$  L/h, it decreases until reached 0.98. This drop in efficiency could be resulting from the large streams of injected bubbles that escape from the thermal boundary layer, resulting in cooling the hot plates' wall surfaces. Thus, we can notice that as HTR increases and at the same time  $\dot{S}_{gen}$  decreases the value of  $\eta_{W-S}$  tends to approach unity. Moreover, the injected air into CWS shows its great energetic and exergetic performance than in HWS.

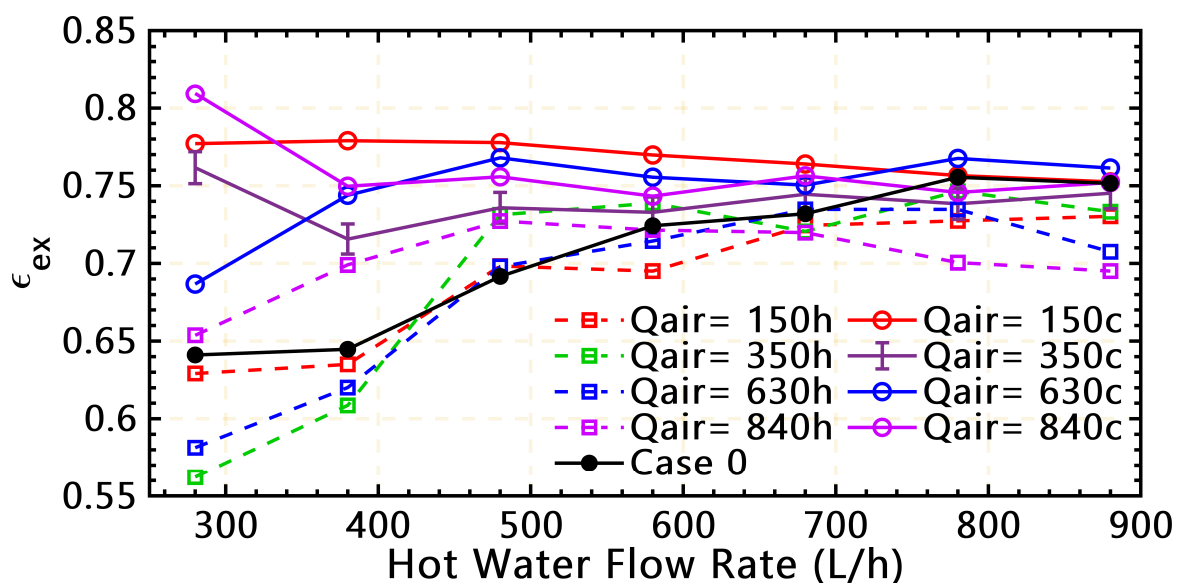


Figure 12. Relationship between  $\epsilon_{ex}$  and  $Q_h$  for original case and, different ABI into both CWS and HWS.

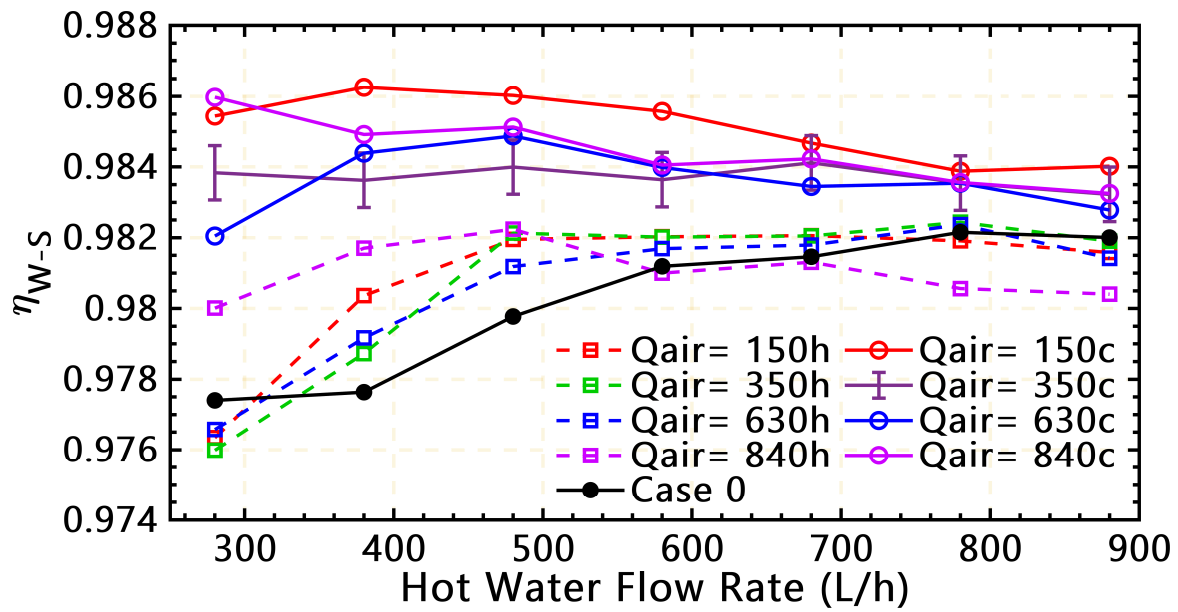


Figure 13. The variations of  $\eta_{W-S}$  at different  $Q_h$  and  $Q_{air}$  at different operating conditions.

4.4. Thermo-Economic Analysis

This section discusses the consequences of using the ABI as a performance enhancement technique for the economical purpose that is defined as [12,32]

$$\eta_P = \frac{NP}{\dot{Q}_c \tau} \tag{32}$$

with

$$NP = \tau (\epsilon_t \Delta E_t - \epsilon_f \Delta E_f) - CRF \times [I_o - SV \times WF] \tag{33}$$

and

$$CRF = \frac{i}{[1 - (1 + i)^{-n}]} \tag{34}$$

Table 3 provides a list of the values utilized in this assessment.

Table 3. The thermo-economic analysis list of parameters.

Symbol	Value
$\tau$	7200 h
$i$	13%
$I_o$	1950 USD
$SV$	0 USD
$n$	23 years
$\epsilon_t$	$3.338 \times 10^{-8}$ USD/J

The net profit per unit transfer load ( $\eta_P$ ) values depicted in Figure 14 for ABI into HWS exhibit competitive advantage at lower values of  $Q_{air}$  and  $Q_h$  for case 150h that reaches 0.35 USD/kJ. This value corresponds to a maximum value of  $\dot{E}x_{des}$  of 0.4 kW. In addition, a noticeable increase in  $\eta_P$  corresponds to case 630h at high  $Q_h$  that also corresponds to a large  $\dot{E}x_{des}$  as it is a function in  $NP$ , this could be due to irreversibility in the system and slug flow that occurs to PHE two-phase flow and cannot be observed experimentally [18]. In general, all the tests condition has positive values which indicate that ABI is economically beneficial.

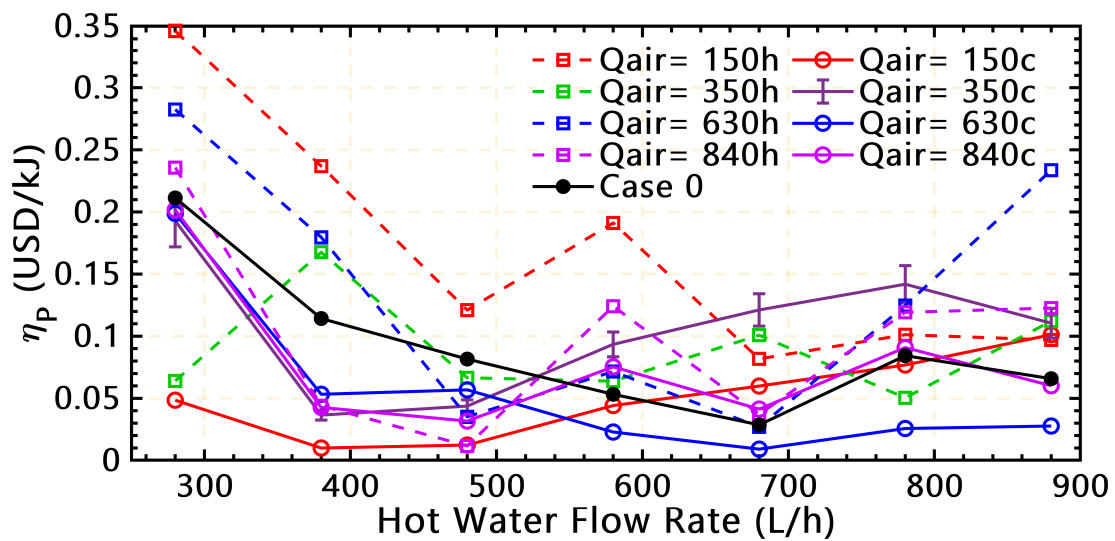


Figure 14.  $\eta_p$  vs. hot water flow rate at different operating conditions.

#### 4.5. Energy and Exergy Effectiveness Optimization

In order to provide a favorable compromise between the energetic and exergetic performance analysis of the C-PHE, Figure 15a demonstrates the  $\epsilon$  and  $\epsilon_{ex}$ . It was noticed that the thermal effectiveness approaches unity for ABI into CWS. Additionally, there are considerable effects at HWS that have maximum values for both thermal and exergy effectiveness. Figure 15b illustrates the dominated and non-dominated solutions of the Pareto front. Air bubbles injected into HWS are favorable in terms of  $\epsilon_{ex}$ , whereas ABI into CWS is superior in terms of  $\epsilon$ .

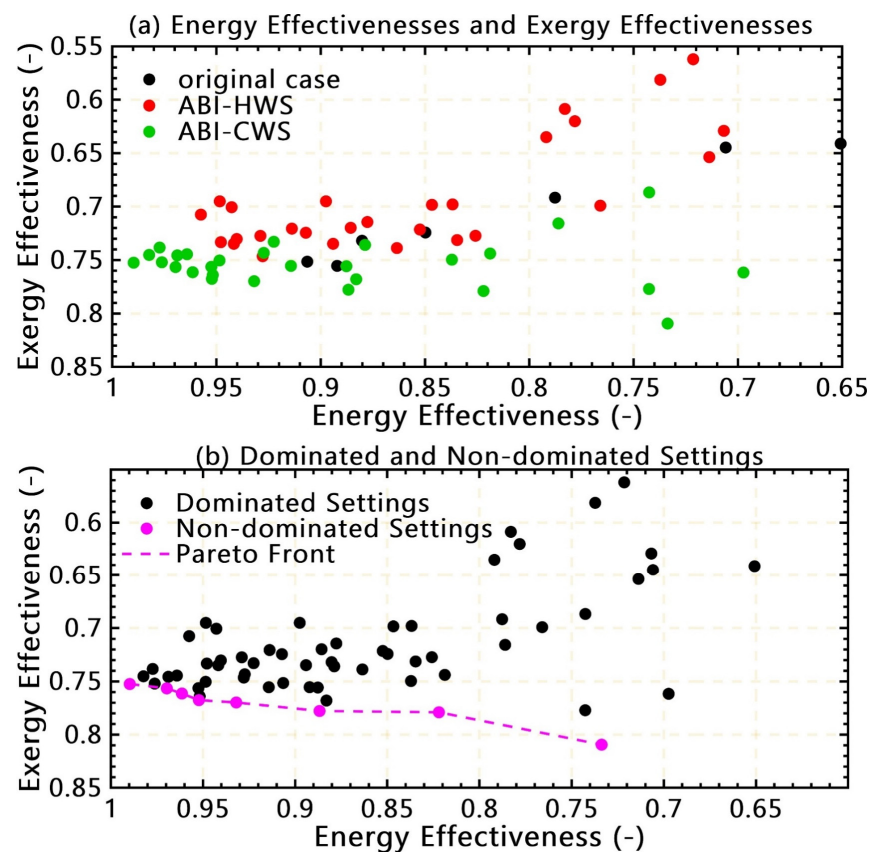


Figure 15. Pareto-front of  $\epsilon$  vs.  $\epsilon_{ex}$  at different operating conditions.

## 5. Conclusions

This paper highlighted the impacts of ABI as a promising technique for enhancing the combined energetic-exergetic performance of a C-PHE by comparing injecting air bubbles into both CWS and HWS under the same operating conditions as the previously published work [12]. Heated water was studied in seven different flow rates with equivalent channels Reynolds number ( $Re_{ch}$ ) of 391, 530, 670, 809, 949, 1088, and 1227. Moreover, a fixed hot temperature and cold-water stream of 50 °C and 290 L/h corresponded to  $Re_{ch}$  of 224, respectively.

The study's main contributions are summarized as follows:

- The effectiveness of C-PHE increases as the NTU increases with the maximum values of 2.996 and 2.219 for counter-flow and parallel flow configurations respectively, for the original case.
- Injecting air bubbles has significant effects in enhancing the NTU by 59% at  $Q_{air}$  of 840 L/h and  $Q_h$  of 380 L/h for CWS.
- The effectiveness reached its maximum value of 0.989 at  $Q_h$  of 880 L/h for CWS which tends to be unity compared to  $\varepsilon$  of 0.957 at  $Q_{air} = 630$  L/h and  $Q_h = 880$  L/h for HWS.
- The effectiveness ratio was enhanced by 18.6% at  $Q_{air}$  of 840 L/h and  $Q_h$  of 880 L/h, for the case of ABI into CWS.
- ABI for C-PHE with counter flow arrangement has remarkable values of NTU and effectiveness compared with parallel flow arrangement for all the tested conditions.
- Injecting air bubbles reduces the  $\dot{S}_{gen}$  and  $N_{s,aug}$  to 0.038 W/K and 0.087, respectively, at  $Q_{air}$  of 150 L/h and  $Q_h$  of 380 L/h into CWS, which enhanced the  $\eta_{W-S}$  to a noticeable increase of 98.6% as a result of EGM.
- Injecting air with a counterflow configuration of C-PHE has a maximum value of  $\eta_{W-S}$  compared with parallel flow arrangement.
- Injecting air enhanced the exergy effectiveness with a maximum value of 80.9% at  $Q_{air}$  of 840 L/h and  $Q_h$  of 280 L/h into CWS compared to 0.774 at the same operating conditions in the case of ABI into HWS.
- Case 150c of ABI-CWS has the best combined energetic-exergetic performance, which has maximum and stable values of  $\eta_{W-S}$  and  $\varepsilon_{ex}$  among all the tested conditions at different operating conditions.
- The positive effects of ABI have been noticed for all the tested conditions for HWS and CWS in the net profit value that reached a maximum value of that reaches 0.35 USD/kJ.

This comprehensive study shows the great effects of ABI as a performance enhancement technique for C-PHE with no need to reinstall or retrofit the original system. Remarkable results were obtained in the case of air bubbles injection into CWS.

**Supplementary Materials:** The following supporting information can be downloaded at: <https://www.mdpi.com/article/10.3390/en16031164/s1>.

**Author Contributions:** Z.M.M.: Conceptualization, Methodology, Software, Validation, Formal analysis, Investigation, Data Curation, Visualization, Writing - Original Draft, Writing—Review & Editing, Resources. M.A.F.: Writing—Review & Editing, Supervision. All authors have read and agreed to the published version of the manuscript.

**Funding:** This research received no external funding.

**Data Availability Statement:** The authors confirm that the data supporting the findings of this study are available within the article and supplementary materials.

**Conflicts of Interest:** The authors declare that they have no known competing financial interests or personal relationships that could have appeared to influence the work reported in this paper.

**Nomenclature****Abbreviations**

ABI	Air bubbles injection
CBW	Cold bench water
C-PHE	Corrugated plate heat exchanger
CWS	Cold water side
EGM	Entropy generation minimization
HBW	Hot bench water
HE	Heat exchanger
HTR	Heat transfer rate
HWS	Hot water side
LM	Logarithmic mean temperature difference
NTU	Number of heat transfer units
PHE	Plate heat exchanger

**English symbols**

$A$	Heat transfer area ( $m^2$ )
$b$	Corrugation depth (m)
$C$	Heat capacity (W/K)
$c$	Specific heat capacity (J/kg.K)
$CRF$	Capital recovery factor (-)
$E_t$	Thermal exergy gain (J)
$E_f$	Friction exergy lost (J)
$Ex_{des}$	Exergy destruction rate (W)
$H$	Total height (m)
$i$	Interest rate (%)
$I_o$	Initial cost (USD)
$L_w$	Total width (m)
$\dot{m}$	Mass flow rate (kg/s)
$N$	Number of plates (-)
$n$	Lifetime (year)
$NP$	Net profit (USD)
$Nu$	Nusselt number (-)
$N_s$	Entropy generation number (-)
$N_{s,aug}$	Augmentation entropy generation number (-)
$P$	Pressure (Pa)
$Q$	Volume flow rate (L/h)
$\dot{Q}$	Heat transfer rate (W)
$SV$	Salvage value (USD)
$\dot{S}_{gen}$	Entropy generation rate (W/K)
$T$	Temperature ( $^{\circ}C$ )
$U$	Overall heat transfer coefficient ( $W/m^2.K$ )
$WF$	Worth capital factor (-)

**Greek symbols**

$\varepsilon$	Effectiveness (%)
$\varepsilon_{ex}$	Exergy effectiveness (%)
$\varepsilon_f$	Cost of each unit per friction exergy (USD/J)
$\varepsilon_t$	Cost of each unit per thermal exergy (USD/J)
$\eta_P$	net profit per unit transfer load (USD/kJ)
$\eta_{W-S}$	Witte-Shamsundar efficiency (%)
$\tau$	Annual operating time (s)
$\omega$	Uncertainty (%)
$\mu$	Dynamic viscosity (kg/m.s)

**Subscripts**

<i>air</i>	Air
<i>act</i>	Actual
<i>aug</i>	Augmentation
<i>avg</i>	Average

<i>c</i>	Cold fluid
<i>ch</i>	Channel
<i>a</i>	Ambient
<i>h</i>	Hot fluid
<i>i</i>	Inlet, Initial
<i>max</i>	Maximum
<i>min</i>	Minimum
<i>o</i>	Outlet
<i>p</i>	Plate
<i>gen</i>	Generation
<i>sp</i>	Single-phase fluid flow
<i>tp</i>	Two-phase fluid flow
<i>t</i>	Total

## References

1. Khan, T.S.; Khan, M.S.; Ayub, Z.H. Single-Phase Flow Pressure Drop Analysis in a Plate Heat Exchanger. *Heat Transf. Eng.* **2017**, *38*, 256–264. [\[CrossRef\]](#)
2. Faizal, M.; Ahmed, M.R. Experimental studies on a corrugated plate heat exchanger for small temperature difference applications. *Exp. Therm. Fluid Sci.* **2012**, *36*, 242–248. [\[CrossRef\]](#)
3. Alzahran, S.; Islam, M.; Saha, S. A thermo-hydraulic characteristics investigation in corrugated plate heat exchanger. *Energy Procedia* **2019**, *160*, 597–605. [\[CrossRef\]](#)
4. Attalla, M.; Maghrabie, H.M. Investigation of effectiveness and pumping power of plate heat exchanger with rough surface. *Chem. Eng. Sci.* **2020**, *211*, 115277. [\[CrossRef\]](#)
5. Yang, C.Y.; Lin, Y.H.; Lin, F.C. Effect of flow direction for the heat transfer performance of refrigerant R-410A evaporation in a plate heat exchanger. *Heat Transf. Eng.* **2013**, *34*, 1133–1139. [\[CrossRef\]](#)
6. Luan, Z.; Zhang, G.; Tian, M.; Fan, M. Flow Resistance and Heat Transfer Characteristics of a New-Type Plate Heat Exchanger. *J. Hydrodyn.* **2008**, *20*, 524–529. [\[CrossRef\]](#)
7. Elbarghthi, A.F.A.; Hdaib, M.Y.; Dvořák, V. Heat Transfer Analysis between R744 and HFOs inside Plate Heat Exchangers. *Entropy* **2022**, *24*, 1150. [\[CrossRef\]](#)
8. Ajeeb, W.; Thieleke da Silva, R.R.S.; Sohel Murshed, S.M. Experimental investigation of heat transfer performance of Al2O3 nanofluids in a compact plate heat exchanger. *Appl. Therm. Eng.* **2023**, *218*, 119321. [\[CrossRef\]](#)
9. Çuhadaroğlu, B.; Hacisalihoğlu, M.S. An experimental study on the performance of water-based CuO nanofluids in a plate heat exchanger. *Int. Commun. Heat Mass Transf.* **2022**, *137*, 106255. [\[CrossRef\]](#)
10. Ham, J.; Kim, J.; Cho, H. Theoretical analysis of thermal performance in a plate type liquid heat exchanger using various nanofluids based on LiBr solution. *Appl. Therm. Eng.* **2016**, *108*, 1020–1032. [\[CrossRef\]](#)
11. Bhattad, A.; Sarkar, J.; Ghosh, P. Energetic and Exergetic Performances of Plate Heat Exchanger Using Brine-Based Hybrid Nanofluid for Milk Chilling Application. *Heat Transf. Eng.* **2020**, *41*, 522–535. [\[CrossRef\]](#)
12. Marouf, Z.M.; Fouad, M.A.; Hassan, M.A. Experimental investigation of the effect of air bubbles injection on the performance of a plate heat exchanger. *Appl. Therm. Eng.* **2022**, *217*, 119264. [\[CrossRef\]](#)
13. Zarei, A.; Seddighi, S.; Elahi, S.; Örlü, R. Experimental investigation of the heat transfer from the helical coil heat exchanger using bubble injection for cold thermal energy storage system. *Appl. Therm. Eng.* **2022**, *200*, 117559. [\[CrossRef\]](#)
14. Marzouk, S.; Al-Sood, M.A.; El-Fakharany, M.K.; El-Said, E.M. Thermo-hydraulic study in a shell and tube heat exchanger using rod inserts consisting of wire-nails with air injection: Experimental study. *Int. J. Therm. Sci.* **2021**, *161*, 106742. [\[CrossRef\]](#)
15. Asano, H.; Takenaka, N.; Fujii, T.; Maeda, N. Visualization and void fraction measurement of gas-liquid two-phase flow in plate heat exchanger. *Appl. Radiat. Isot.* **2004**, *61*, 707–713. [\[CrossRef\]](#) [\[PubMed\]](#)
16. Buscher, S. Digital Image Analysis of Gas-Liquid Flow in a Cross-Corrugated Plate Heat Exchanger Channel: A Feature-Based Approach to Quantify the Impact of Two-Phase Distribution and Flow Direction on Flow Patterns. *SSRN Electron. J.* **2022**, *154*, 104149. [\[CrossRef\]](#)
17. Buscher, S. Two-phase pressure drop and void fraction in a cross-corrugated plate heat exchanger channel: Impact of flow direction and gas-liquid distribution. *Exp. Therm. Fluid Sci.* **2021**, *126*, 110380. [\[CrossRef\]](#)
18. Buscher, S. Visualization and modelling of flow pattern transitions in a cross-corrugated plate heat exchanger channel with uniform two-phase distribution. *Int. J. Heat Mass Transf.* **2019**, *144*, 118643. [\[CrossRef\]](#)
19. Lee, D.; Song, K.S.; Yun, S.; Kim, Y. Experimental evaluation of single- and two-phase pressure drops through inlet and outlet ports in a plate heat exchanger. *Int. J. Heat Mass Transf.* **2020**, *158*, 120009. [\[CrossRef\]](#)
20. Pandey, S.D.; Nema, V.K. An experimental investigation of exergy loss reduction in corrugated plate heat exchanger. *Energy* **2011**, *36*, 2997–3001. [\[CrossRef\]](#)
21. Al Zahrani, S.; Islam, M.S.; Saha, S.C. Heat transfer enhancement of modified flat plate heat exchanger. *Appl. Therm. Eng.* **2021**, *186*, 116533. [\[CrossRef\]](#)

22. Yilmaz, M.; Sara, O.; Karsli, S. Performance evaluation criteria for heat exchangers based on second law analysis. *Exergy Int. J.* **2001**, *1*, 278–294. [[CrossRef](#)]
23. Khorasani, S.; Moosavi, A.; Dadvand, A.; Hashemian, M. A comprehensive second law analysis of coil side air injection in the shell and coiled tube heat exchanger: An experimental study. *Appl. Therm. Eng.* **2019**, *150*, 80–87. [[CrossRef](#)]
24. Tiwari, A.K.; Tiwari, P.; Sarkar, J. Combined energy and exergy analysis of a corrugated plate heat exchanger and experimental investigation. *Int. J. Exergy* **2014**, *15*, 395. [[CrossRef](#)]
25. Khorasani, S.; Dadvand, A. Effect of air bubble injection on the performance of a horizontal helical shell and coiled tube heat exchanger: An experimental study. *Appl. Therm. Eng.* **2017**, *111*, 676–683. [[CrossRef](#)]
26. Bejan, A. *Advanced Engineering Thermodynamics*; John Wiley & Sons Inc.: Hoboken, NJ, USA, 2016. [[CrossRef](#)]
27. Witte, L.C.; Shamsundar, N. A Thermodynamic Efficiency Concept for Heat Exchange Devices. *J. Eng. Power* **1983**, *105*, 199–203. [[CrossRef](#)]
28. Sinaga, N.; Khorasani, S.; Nisar, K.S.; Kaood, A. Second law efficiency analysis of air injection into inner tube of double tube heat exchanger. *Alex. Eng. J.* **2021**, *60*, 1465–1476. [[CrossRef](#)]
29. Bejan, A. Entropy generation optimization: The new thermodynamics of finite-size devices and finite-time processes. *J. Appl. Phys.* **1996**, *79*, 1191. [[CrossRef](#)]
30. Moffat, R.J. Describing the uncertainties in experimental results. *Exp. Therm. Fluid Sci.* **1988**, *1*, 3–17. [[CrossRef](#)]
31. Donoghue, D.; Albadawi, A.; Delauré, Y.; Robinson, A.; Murray, D. Bubble impingement and the mechanisms of heat transfer. *Int. J. Heat Mass Transf.* **2014**, *71*, 439–450. [[CrossRef](#)]
32. Zhou, X.; Bai, H.; Xu, Q.; Mansir, I.B.; Ayed, H.; Abbas, S.Z.; Mahariq, I.; Jarad, F. Evaluations on effect of volume fraction of injected air on exergo-economic performance of a shell and tube heat exchanger. *Case Stud. Therm. Eng.* **2022**, *35*, 101919. [[CrossRef](#)]

**Disclaimer/Publisher's Note:** The statements, opinions and data contained in all publications are solely those of the individual author(s) and contributor(s) and not of MDPI and/or the editor(s). MDPI and/or the editor(s) disclaim responsibility for any injury to people or property resulting from any ideas, methods, instructions or products referred to in the content.